

# Determination of rolling element bearing condition via acoustic emission

A Cockerill<sup>1</sup>, A Clarke<sup>1</sup>, R Pullin<sup>1</sup>, T Bradshaw<sup>2</sup>, P Cole<sup>2</sup>  
and KM Holford<sup>1</sup>

Proc IMechE Part J:  
J Engineering Tribology  
2016, Vol. 230(11) 1377–1388  
© IMechE 2016

Reprints and permissions:  
sagepub.co.uk/journalsPermissions.nav  
DOI: 10.1177/1350650116638612  
pij.sagepub.com



## Abstract

Acoustic emission is an emerging technique for condition monitoring of rolling element bearings and potentially offers advantages for detection of incipient damage at an early stage of failure. Before such a technique can be applied with confidence for health monitoring, it is vital to understand the variation of acoustic emission generation with operating conditions in a healthy bearing. This paper investigates the effects of increased speed and load on the generation of acoustic emission within cylindrical roller bearings, and it was found that the root mean square signal level increased significantly with increasing speed whereas increasing load had a far weaker effect. The  $AE_{RMS}$  value for each experiment was compared with the trend of the  $\Lambda$  value. The bearing was operating under full film lubrication regime, so it was determined that increases in  $AE_{RMS}$  were not caused by asperity contact. By consideration of trends in frequency energy amplitude, it was determined that excitation of the bearings resonant frequencies were responsible for an increase of energy in the frequency range of 20–60 kHz. The excitation energy at 330 kHz (the acoustic emission sensor's resonant frequency) increased with load, indicating a link between high-frequency emission and stress at the contact zone. Following characterisation of the bearing under normal operating conditions, an accelerated life test was conducted in order to induce fatigue failure. The frequency response demonstrated that throughout a period of constant wear, the energy amplitude at the bearings resonant frequency increased with time. As the bearing failure became more significant, the energy of the high-frequency components above 100 kHz was spread over a broader frequency range as multiple transient bursts of energy were released simultaneously by fatigue failure of the raceways. This paper demonstrates the potential of acoustic emission to provide an insight into the bearing's behaviour under normal operation and provide early indication of bearing failure.

## Keywords

Rolling element bearings, condition monitoring, acoustic emission, damage, frequency

Date received: 28 August 2015; accepted: 17 February 2016

## Introduction

Rotating machinery is a broad term used to cover the mechanical systems increasingly used and heavily relied upon within modern society. All dominant industry sectors, including aerospace, automotive and power generation, require their assets or products to perform efficiently and reliably, especially when the failure of such machinery could result in the loss of human life. Operators, therefore, continue to adopt advanced pro-active maintenance strategies, rather than undertaking costly reactive maintenance.<sup>1</sup> This paper focuses specifically on the health monitoring of rolling element bearings. The degradation of a rolling element bearing depends largely on the operating conditions. Overloading, lack of lubrication, improper assembly and misalignment are all common causes of bearing failure. When a bearing is operated under controlled conditions; however, failure is often due to rolling contact fatigue that begins beneath the

contacting surfaces. Sub-surface cracks begin to propagate through the micro-structure, making their way to the surface leading to the removal of small pieces of material, otherwise known as pitting.<sup>2</sup> Early condition monitoring techniques focussed predominantly on the vibrational response of a mechanical system, relying heavily on the increase in amplitude of the bearing defect frequencies (i.e. the fundamental frequencies at which the various bearing components interact with each other) as damage propagated along the rollers and raceways.<sup>3</sup> In recent

<sup>1</sup>School of Engineering, Cardiff University, Cardiff, UK

<sup>2</sup>Mistras Group Limited, Cambridge, UK

### Corresponding author:

A Cockerill, School of Engineering, Cardiff University,  
Cardiff CF24 3AA, UK.

Email: CockerillA@cardiff.ac.uk

years, research has investigated the application of acoustic emission (AE) to bearing condition monitoring. Whereas traditional vibration transducers are typically sensitive between 0 and 50 kHz, AE sensors operate over a far wider frequency range typically between 20 kHz and 1 MHz. As a result, AE sensors have the ability to detect the transient elastic surface waves associated with the strain energy released during the plastic deformation of materials, by crack initiation and propagation, by frictional sources and throughout the wear process.<sup>4</sup>

Initial AE analysis of rolling element bearings demonstrated an increased sensitivity to increases in the bearing defect frequencies so commonly used in vibrational analysis.<sup>5</sup> Although the bearing defect frequencies commonly exist below 1 kHz, the frequency content of each 'burst', created as a roller passes over a defect, has been seen to exceed 100 kHz enabling its detection through AE. When combined with the fact that AE operates in a frequency band outside of the typical mechanical noise frequency range, it has been shown that AE has a much greater sensitivity to incipient bearing defects when compared to vibration due to its enhanced signal to noise ratio.

AE is a passive form of damage detection, with the high-frequency elastic stress waves exciting a piezoelectric crystal in the sensor and hence producing a voltage. When used in static testing, such as a tensile fatigue test, it is common practice to see long periods of inactivity with AE activity only occurring during crack growth as the peak amplitude of the emitted waves exceed the user defined threshold within the AE system. This is commonly referred to as 'burst-type' emission. The AE signal produced by rotating machinery is defined as 'continuous' emission as when the raw signal is viewed, a number of transients are witnessed in quick succession. Research into the influence of rotational speed and applied load on the AE signal of rolling element bearings has demonstrated that the rotational speed has a much greater effect when compared with applied load.<sup>6-8</sup> Choudhury and Tandon<sup>7</sup> concluded that the increase in the AE parameters studies was due to the increase in dynamic stresses caused by the increased rotational speed. Couturier and Mba<sup>6</sup> studied the effect of the Lambda ratio,  $\Lambda$ , on the AE signal of a roller bearing operating under boundary and mixed lubrication regimes ( $0.3 < \Lambda < 3$ ). It was determined by the authors that the continuous emission of AE was due to asperity contact within the contact area. The rise in  $AE_{RMS}$  with respect to speed was attributed to the increase in the frequency of occurrence of asperity contacts whilst operating under low  $\Lambda$  values, i.e.  $\Lambda < 1$ . It was also shown that as  $\Lambda$  increases the magnitude of  $AE_{RMS}$  begins to decrease, however, the effect of full fluid film lubrication was not investigated in their study.

Graney and Starry<sup>9</sup> determined that a bearings resonant frequency can be used to determine the

condition of the bearing throughout its life. Described as the high-frequency natural bearing resonance indicators (HFNBRI's), the region between 3 and 50 kHz is shown to be excited with increasing speed as well as during the increase of friction and wear with the contact zone. Using traditional accelerometers, Graney and Starry<sup>9</sup> were able to determine the stage of wear of multiple industrial pumps through a combination of the HFNBRI's and the bearing defect frequencies.

Previous work by the authors of this paper demonstrated the sensitivity of AE to the detection of very small artificial defects engraved on the outer raceway.<sup>10</sup> It was found that the presence of defects caused an increase in the frequency response at around 100 kHz. In addition to this, there was also found to be an increase in the frequency range of 25–60 kHz as the defect was artificially enlarged from a point defect to a line defect.

This paper aims to study the effect that both speed and load have independently upon the AE signal in order to determine the true cause of the increase in AE amplitude with respect to speed in rolling element bearings, under a full film lubrication regime. This was investigated through a series of controlled bearing tests, first ramping the speed up and down under a range of loads, and vice versa, ramping the load under various speeds. The data collected were then analysed using the root mean square (RMS) value as well the frequency spectrum examined with respect to time. Once the effect of speed and load had been established, an accelerated life test was also conducted to determine the effect of naturally growing damage on the AE signal.

## Experimental procedure

The test bearing, a single-row roller bearing, type SKF N204ECP, was mounted on a shaft supported by two double-row tapered roller bearings, type SKF N22205/20E, with a 10:1 lever arm used to apply a radial load to the test bearing (Figure 1).

Each bearing was lubricated with a commonly used mineral gearbox oil meeting performance specification OEP-80<sup>11</sup> through individual oil jets at a sump temperature of 50°C. To determine the individual roller loads on each rolling element within the bearing, the method of Harris and Kotzalas<sup>12</sup> was used. This technique is complex but yields details information of the load distribution within the bearing. An initial radial displacement of the loaded raceway is assumed, and from this displacement and the bearing geometry, the displacement at each roller location is calculated. Hertzian contact mechanics is then used to determine the load at each roller necessary to cause this displacement (as the sum of the elastic displacements at the inner and outer raceway contacts), and these individual roller loads are summed to give the overall bearing load. Based on the calculated bearing load,

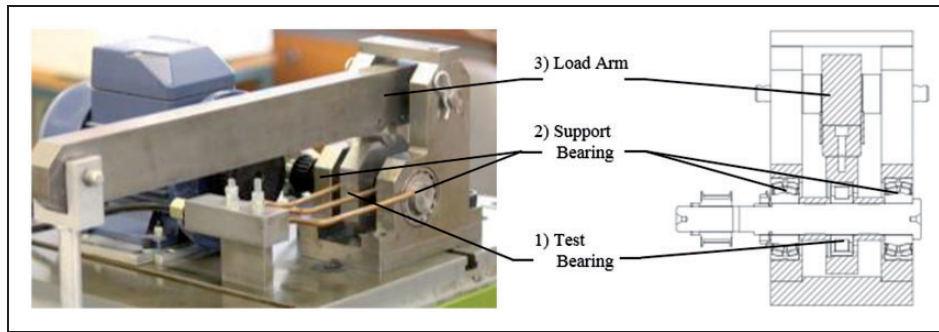


Figure 1. Test head schematic.

Table 1. Equivalent bearing load.

Applied mass (kg)	Bearing load (N)	Maximum Hertzian stress (MPa)	Maximum roller load (N)
0	304	673	194.29
5	794	954	390.99
10	1285	1142	559.82
15	1775	1291	715.86
20	2266	1419	864.21

the assumed radial displacement is adjusted iteratively until the calculated bearing load is equal to the applied radial load. This process produces a converged set of roller loads for the bearing, from which the maximum roller load may be determined. Due to the nature of this calculation, a computational code was written to perform the calculations reported in this paper. Following calculation of maximum roller load, the Hertzian contact half-width,  $a$ , at the more heavily stressed inner-raceway is calculated using

$$a = \sqrt{\frac{4PR}{\pi E^*}} \quad (1)$$

where  $P$  is the load per unit length,  $R$  is the relative radius of curvature and  $E^*$  is the relative elastic modulus.

Finally, the maximum Hertzian contact pressure,  $p_0$ , is calculated using

$$p_0 = \frac{2P}{\pi a} \quad (2)$$

The contact fatigue stress for roller bearing steel is commonly taken as 1500 MPa, and therefore, the applied mass was limited to 20 kg, corresponding to a Hertzian contact stress of 1419 MPa. Table 1 summarises the maximum Hertzian contact stresses for all of the loads applied within this experiment.

Mistras physical acoustics (MPA) Nano30 sensors were applied to the housing of each bearing, as well as a fourth sensor placed on the load arm at the locations in dots in Figure 2. Nano30 sensors were selected because of their small size and are sensitive between 125 and 750 kHz with a resonant frequency of approximately 300 kHz. By placing AE sensors on

the housing of each bearing, it is easier to distinguish between external AE sources and those originating from within the bearing. The sensors were bonded to the bearing housings using Loctite 5980 silicon, and the quality of the bond was determined by standard techniques involving making pencil lead breaks close to the sensor, commonly known as a Hsu-Nielson source.<sup>13,14</sup> The stress wave produced by a pencil lead break is highly repeatable and allows the effectiveness of the acoustic coupling between sensor and bearing housing to be established prior to testing.

Each sensor was connected to a MPA 2/4/6 pre-amplifier, with a gain of 40 dB and a band-pass filter of 20–1200 kHz. From the pre-amplifier, the signal was passed into a MPA PCI-2 system where hit-based and time-based AE parametrics are recorded within a data file. A National Instruments (NI) USB 6008 data acquisition unit were used in conjunction with NI LabView software, to record the bearing temperature, oil bath temperature, average speed and applied load. In addition to this, NI LabView was used to trigger the MGL PCI-2 system to record a wavestream (the acquisition of the raw AE signal independent of threshold for a period of time) at user-defined intervals.

The measured bearing temperature was used to determine the oil viscosity at ambient pressure ( $\eta_0$ ) and the pressure coefficient of viscosity ( $\alpha$ ), which when combined with the operating speed, roller/raceway contact geometry, material properties and the applied load allowed for the calculation of the minimum elastohydrodynamic fluid film thickness within the contact zone using the well-known Dowson and Higginson formula<sup>15</sup>

$$h_{\min} = 1.6 \frac{\alpha^{0.6} (\eta \bar{u})^{0.7} (E')^{0.03} R^{0.43}}{(w')^{0.13}} \quad (3)$$

where  $\alpha$  is the pressure coefficient of the oil used,  $u$  is the mean speed at the contact,  $E'$  is the relative modulus of elasticity,  $R$  is the relative radius of contacting bodies and  $w'$  is the load per unit length. The oil viscosity,  $\eta$ , is given by

$$\eta = \eta_0 \exp(\alpha p) \quad (4)$$

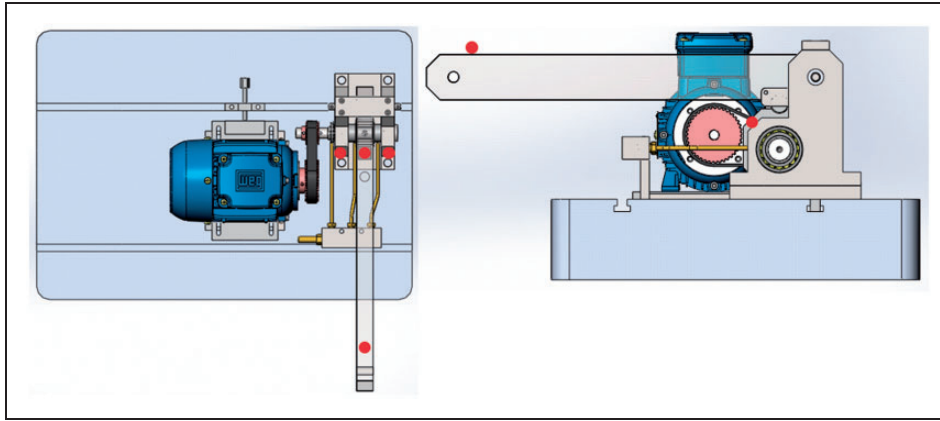


Figure 2. Location of the AE sensors.

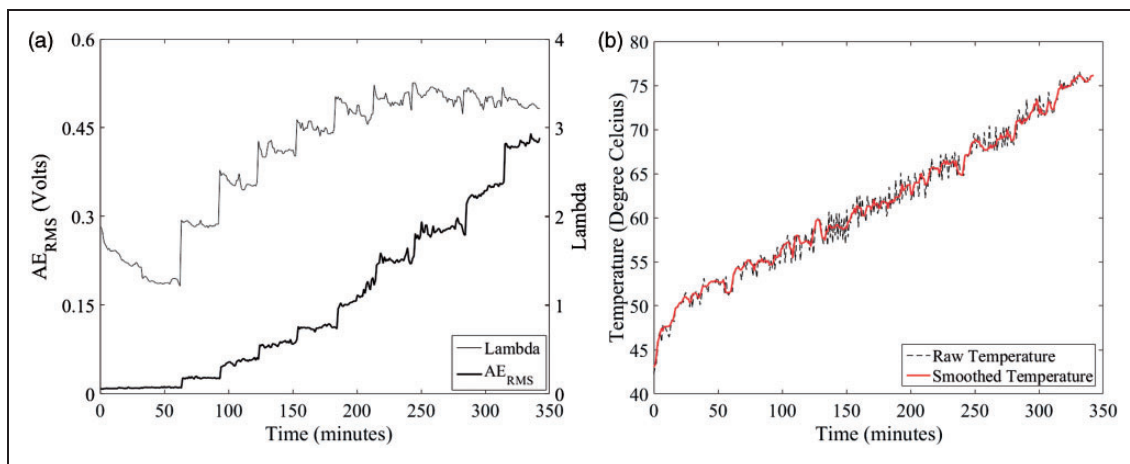


Figure 3. (a) Lambda and AERMS vs. time and (b) corresponding temperatures during run-in test.

A Taylor Hobson Talysurf profilometer was used to measure the RMS surface roughness,  $R_q$ , of the raceway and rolling element which was found to be 0.077 and 0.074  $\mu\text{m}$ , respectively. A composite surface roughness was determined and used with the minimum fluid film thickness at the inner raceway to determine the  $\Lambda$  ratio, which is a commonly used indicator of the lubrication regime within the bearing and is defined as

$$\Lambda = \frac{h_{\min}}{\sqrt{R_{q1}^2 + R_{q2}^2}} \quad (5)$$

where  $R_{q1}$  and  $R_{q2}$  are the surface roughness values,  $R_q$ , of the two contacting bodies.

## Results and discussion

Following the guidelines provided by NSK Europe,<sup>16</sup> a new test bearing was run in. A mass of 5 kg was applied to the load arm, giving a radial load of 794 N at the bearing and the speed was increased from 590 to 5980 r/min in increments of approximately 590 r/min. Each speed stage was held for a

period of 30 min to ensure that the bearing temperature reached steady state conditions. Raw AE signals (wavestreams) were recorded once per minute along with speed, load and bearing temperature. Figure 3 plots both the theoretical Lambda value and  $AE_{RMS}$  against time. It can be seen that as the test starts, the bearing is subject to a mixed lubrication regime, developing later into a full fluid film lubrication regime as the speed is increased. The  $AE_{RMS}$  value is seen to increase with speed despite the bearing having a full fluid film separating the raceway and roller, hence suggesting the increase in  $AE_{RMS}$  is not directly related to asperity contact under these conditions. As the bearing is running in, however, it is likely that some wear or plastic deformation of asperities will be occurring during this experiment as the contacting surfaces are modified.

To better understand the independent influences of speed and load on AE generation, a speed ramp test and a load ramp test were conducted separately following the running-in procedure. The speed ramp test increased the speed from 590 to 5980 r/min and back down to 590 r/min, in steps of 590, 1180, 2380, 3580, 4780 and 5980 r/min with a radial load of 794 N applied to the test bearing. The load ramp increased

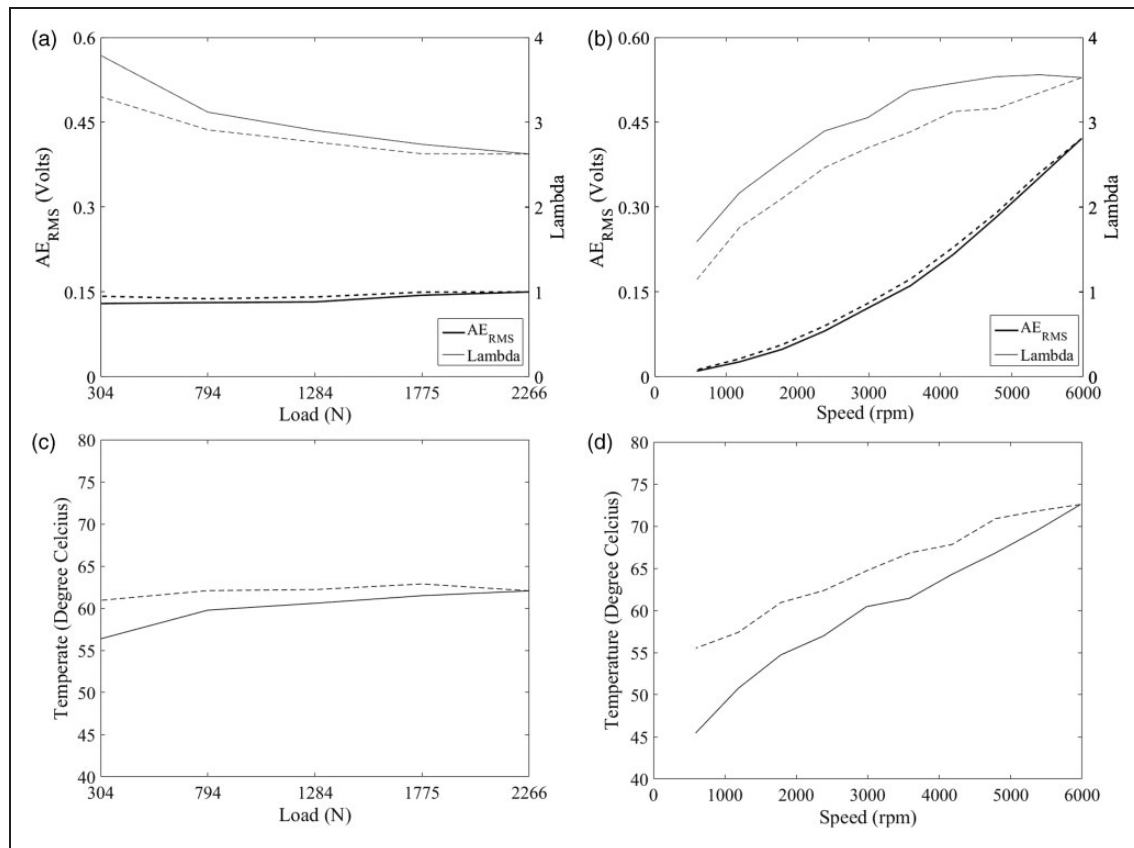


**Figure 4.** Lambda and AERMS vs. (a) load ramp, (b) speed and corresponding temperature vs. (c) load and (d) speed.

the load from 304 N to 2266 N and back down to 304 N in steps of 490 N, at a constant speed of 2980 r/min. Each speed or load increment was held for a period of 10 min, with the wavestream and temperature recorded every minute. Figure 4(a) and (b) shows the RMS values, as well as the corresponding Lambda value, as a function of load and speed, respectively. As the speed is increased under constant load conditions, the  $AE_{RMS}$  increases dramatically whereas for an increase in load at constant speed, the  $AE_{RMS}$  remains relatively constant. In Figure 4, the speed/load increasing phase of the test is plotted with a solid line, whilst the dashed line represents the decreasing phase of the test. For both tests, there is a slight difference between the  $AE_{RMS}$  values for the load/speed increasing and decreasing portions of each test. It is thought that this is due to the reduction in Lambda value as the oil has a slightly higher temperature during the latter stages of the test. It should be noted that the lambda value used relates to the surface roughness of the run-in bearing measured prior to these experiments, as it was not possible to take surface roughness measurements during the tests. However, in the authors' experience, these values are unlikely to change significantly during normal operation of the bearings used for this testing.

To determine the effect of the applied load on the AE generated during speed ramp tests, and vice versa for the effect of speed on the load ramp tests, two

further experiments were conducted, referred to here as 'mixed' tests. The first experiment increased and then decreased the speed under constant loads of 304, 794, 1284, 1775 and 2266 N, respectively, and the second experiment repeated the load ramp test under constant speeds of 590, 1180, 2380, 3580, 4780 and 5980 r/min. For both experiments, wavestreams were recorded every minute for a period of 10 min before the variable being ramped was increased/decreased. Figure 5(a) and (b) illustrate the  $AE_{RMS}$  response for each operating condition during the speed or load increasing phase, demonstrating a strong correlation between speed and  $AE_{RMS}$  which is almost completely independent of load as seen by Choudhury and Tandon.<sup>7</sup>

With a broad relationship between the speed, load and  $AE_{RMS}$  determined, Figure 6(a)–(c) shows the raw wavestreams in order to illustrate the characteristic signal differences at speeds of 590, 2380 and 5980 r/min and a bearing load of 1285 N. Due to the near order of magnitude difference between the amplitudes of each signal as the speed is increased, it is to be noted that the amplitude axis on each figure is not to the same scale. The high-frequency noise floor is a common feature present in each of the figures, albeit at differing amplitudes. At random intervals, there also exist transient bursts of energy, appearing as 'spikes' in the signals. Through comparison of the four channels monitored, the possibility of these

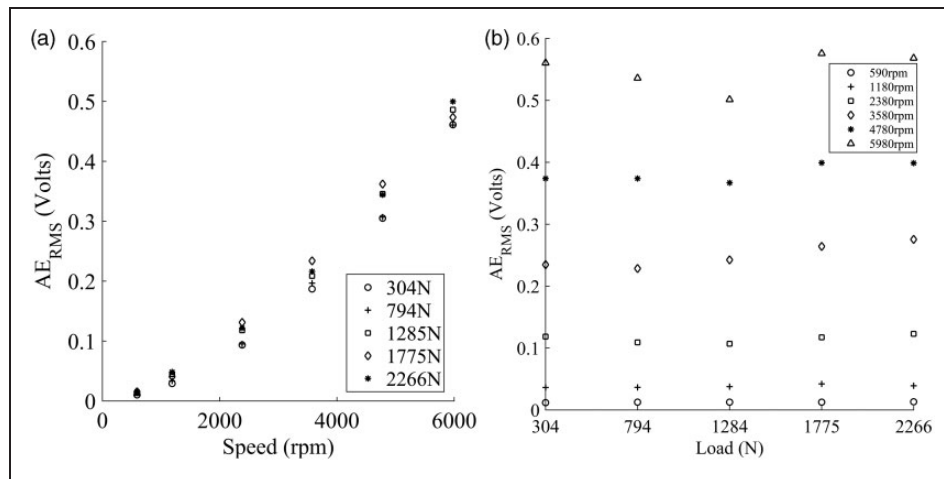


Figure 5. (a) AERMS vs. speed and (b) AERMS vs. load.

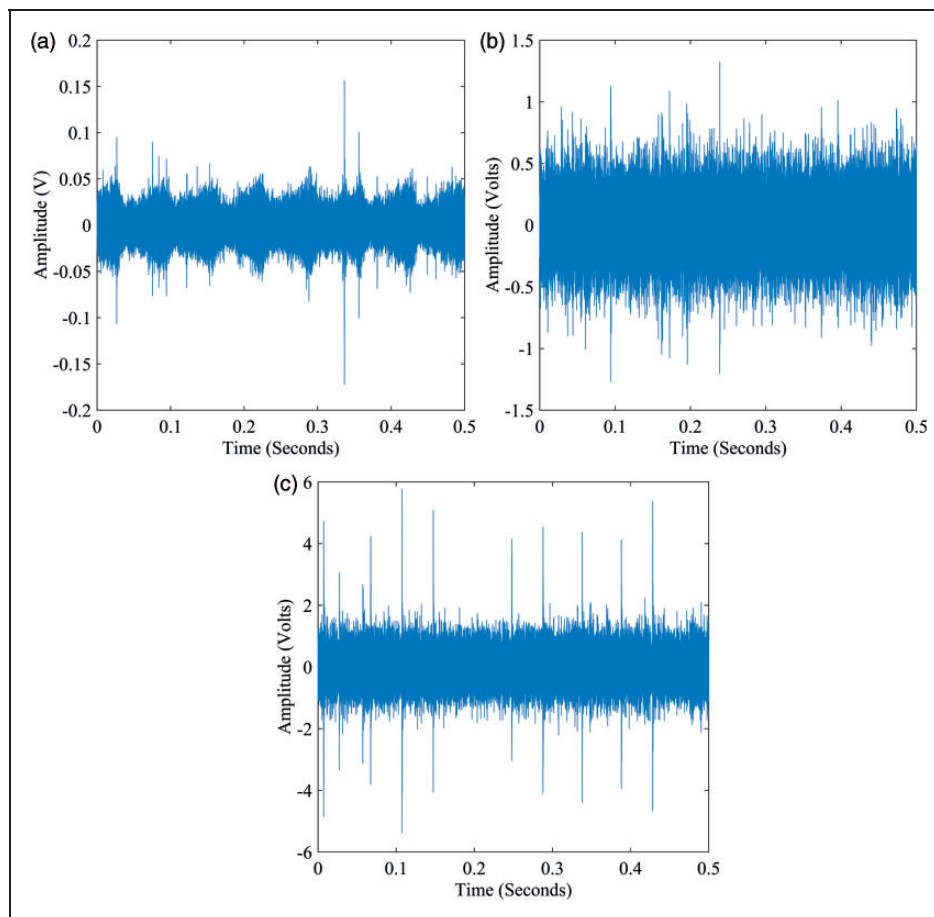
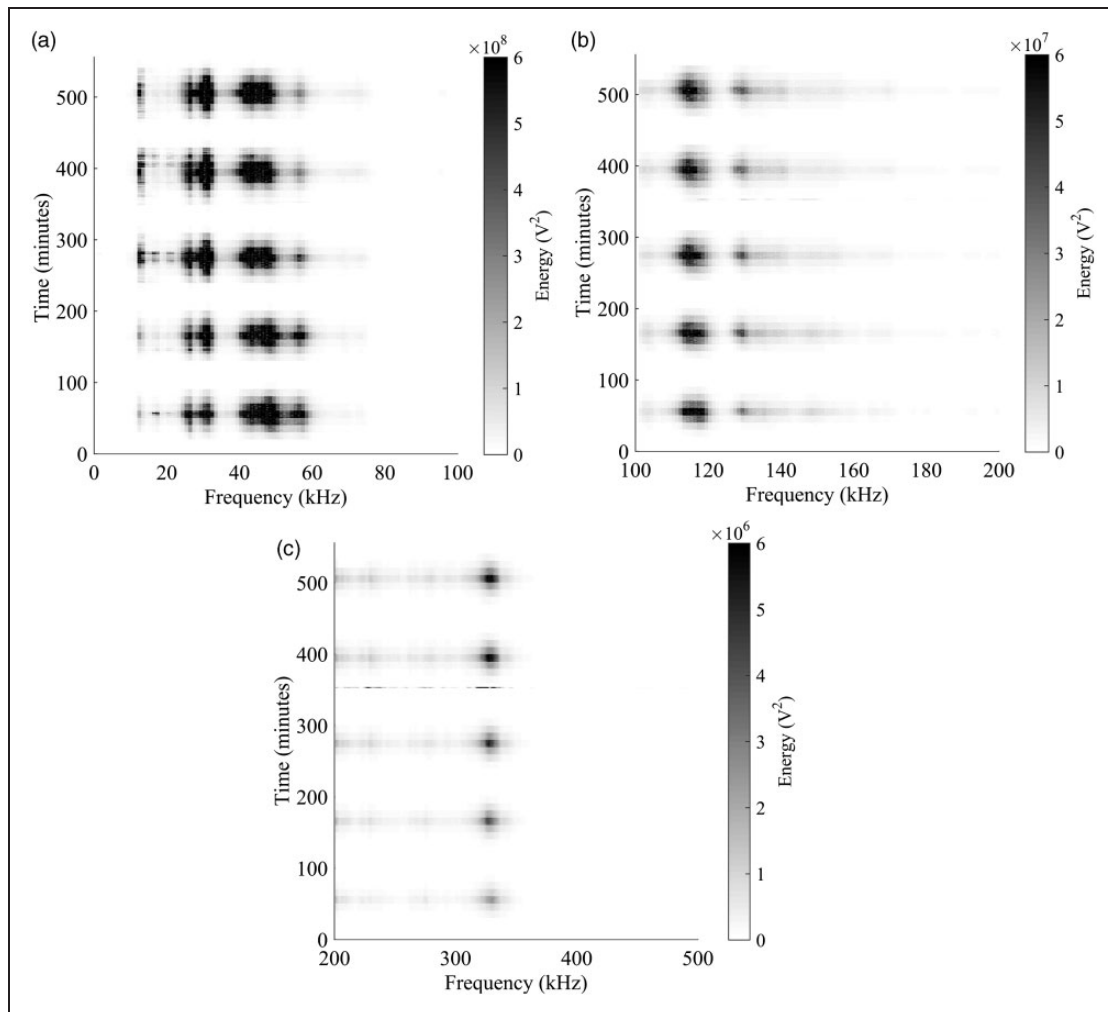


Figure 6. Raw AE waveforms at (a) 590 r/min, (b) 2980 r/min and (c) 5980 r/min.

being electrical noise is ruled out as the transient bursts occur at the sensor mounted on the test bearing and upon the load arm. The attenuation between the test bearing and the two support bearings is far more severe when compared with the attenuation as a signal propagates along the load arm, due to the transmission of the signal through the shaft, inner race and rollers of the support bearings. The true cause of these

transient bursts is unknown, but there are a number of possibilities that may cause increased emission within the test bearing including: the over-rolling of wear debris particles produced during the running in procedure; strain energy released from asperities due to high oil film pressures; asperity contact within the contact zone. Lees et al.<sup>17</sup> illustrated a transient burst within the time-domain and thought it to be the



**Figure 7.** Variation of frequency content of wavestreams with time in the region of (a) 0–100 kHz, (b) 100–200 kHz and (c) 200–500 kHz.

detection of sub-surface cracking emitted from a weakened race cup from a ball bearing.

Within the raw waveforms, it is seen that the continuous emission, which forms most of the signal baseline, also increases in amplitude as the speed increases. To better determine the cause for the increase in amplitude, a Fast Fourier Transform (FFT) was carried out for each of the wavestreams recorded during the experiment. To increase the sensitivity of the results to periodic signals, the frequency range was separated into a number of bins and the calculated power of all the frequencies within each bin were summed.<sup>18</sup> For this experiment, the bin size was set to 1 kHz. Finally, to determine trends in the frequency response, these ‘binned FFTs’ were plotted against time to show the evolution of frequency content over the duration of the mixed testing. Figure 7(a)–(c) are the binned FFTs plotted against time for the data collected during the mixed testing phase, where speed was ramped under different applied loads. Due to the order of magnitude difference in the power spectra in different frequency ranges, Figure 7(a)–(c), divide the broad spectrum of

the data collected in the mixed test (repeated speed ramp with incremented load) into three different frequency bands, 0–100 kHz, 100–200 kHz and 200–500 kHz, respectively, each with different scales for amplitude.

In Figure 7(a), the amplitude of the energy in the region of 25 and 50 kHz increases and decreases as the speed is ramped up and down, respectively, with the repeated burst of high energy signal corresponding to the highest shaft speeds. This corresponds directly with the findings of Graney and Starry<sup>9</sup> indicating that the excitation energy provided through the speed ramps excites the bearing’s resonant frequencies and hence produces the continuous emission seen in the raw signal profiles. This offers a plausible explanation for the increased  $AE_{RMS}$  values with increasing speed. Figure 7(b) exhibits high-excitation energy at 115 kHz and Figure 7(c) shows an increase at 330 kHz, close to the resonant frequency of the AE sensor. Frequency content in these regions is commonly attributed to the strain energy release (often during plastic deformation) and is thought to have been caused by the transients within the raw

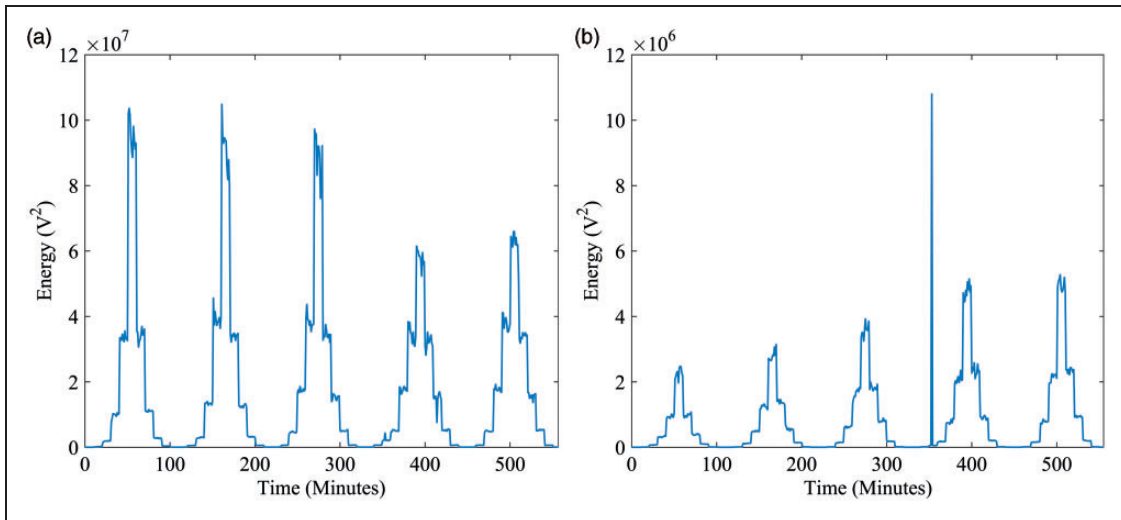


Figure 8. Variation of energy content of signal with time within a frequency bin of (a) 115 kHz and (b) 330 kHz.

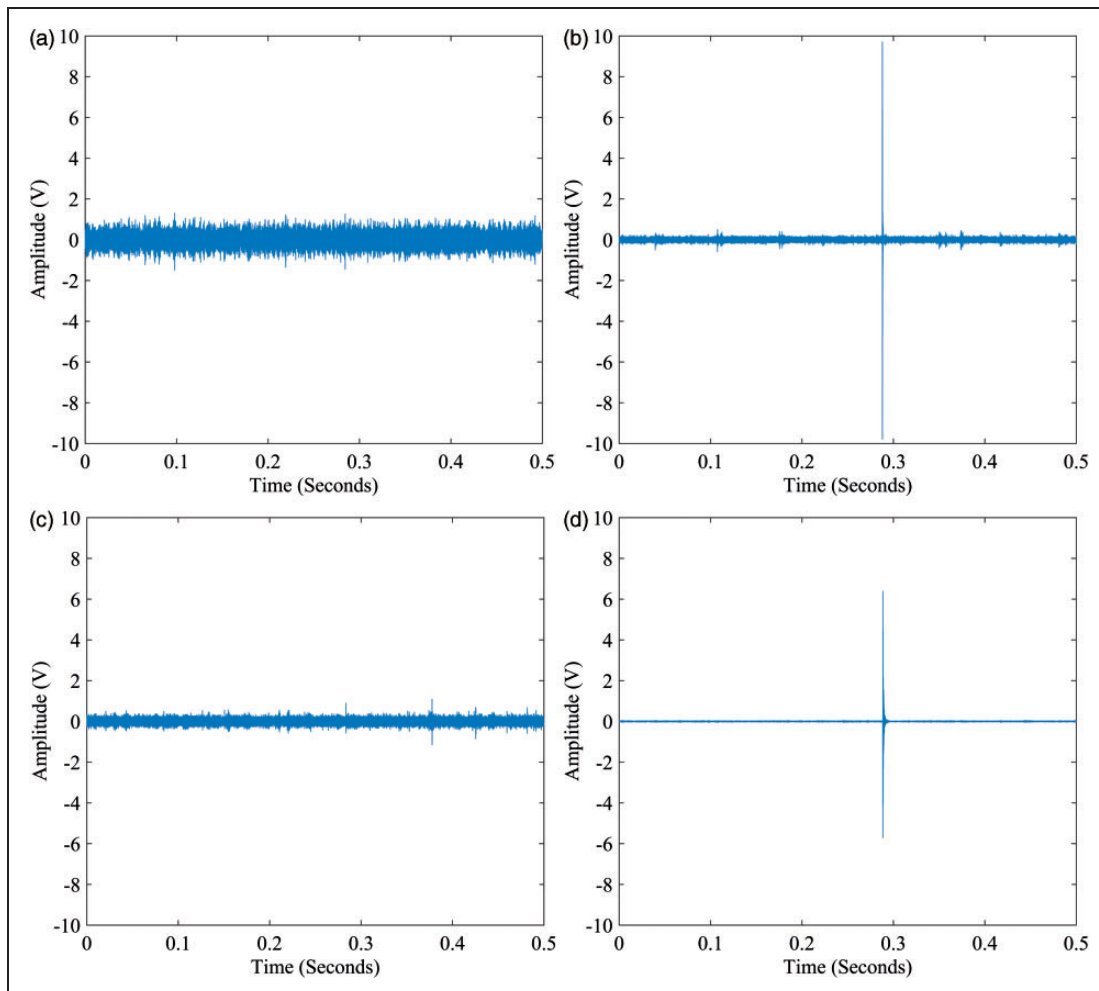
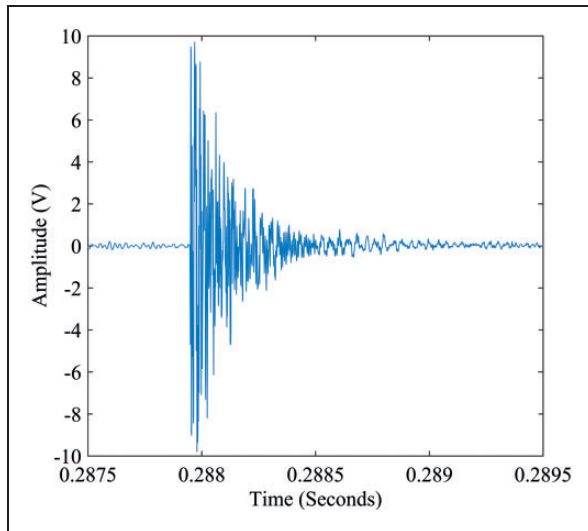


Figure 9. Raw AE waveforms at 353 min from (a) drive end support bearing, (b) test bearing, (c) non-drive end bearing and (d) load arm bearing.

waveforms as discussed earlier. To further understand the amplitude changes in the high-frequency regions, it is possible to plot the variation in energy with time at selected frequencies. Figure 8(a) and (b) are such

plots at 115 and 330 kHz, respectively. Figure 8(a) at 115 kHz shows that as the load is increased in successive repetitions of the speed ramp test the energy within this particular frequency range decreases.



**Figure 10.** Transient burst from the test bearing.

The opposite response is witnessed in Figure 8(b) at 330 kHz. As the load is increased, the energy amplitude increases significantly indicating the influence of increasing load on the frequency response and indicating greater strain energy release within the bearing as the stresses increase with applied load.

Of greater interest in Figure 8(b) is the large peak visible at 353 min, a clear deviation from the trend, particularly as it occurs at a relatively low speed. To help determine the cause of this high peak, Figure 9(a)–(d) are the raw waveforms recorded at each of the four sensor locations at this moment in time. Of immediate interest is the single transient which almost reached  $\pm 10$  V at 0.28 s within the test-bearing signal, shown in more detail in Figure 10. Experience of AE signals suggests that this burst originates from an external source such as a sharp impact as it has the same characteristic appearance as a pencil lead break used to determine how well as sensor is coupled to the surface. The test, however, was run with a sheet steel guard in place, eliminating the possibility of it being an external source. In addition to this, it can be seen that the transient burst originates within the test bearing and is transmitted through the load arm sensor albeit at a lower amplitude due to attenuation. As the signal is attenuating, and is not visible within either of the support bearing signals, an electrical noise spike can also be ruled out. Therefore, the origin of this transient is thought to be due to a change of the running conditions and may be caused by the over-rolling of debris, a foreign particle or possibly caused by some relative motion between the test bearing housing and loading mechanism. Other potential sources include the detection of sub-surface cracking and plastic deformation within the contact zone. However, at a load of 2266 N, the bearing is under the fatigue load limit, therefore, minimising the possibility of this being the cause.

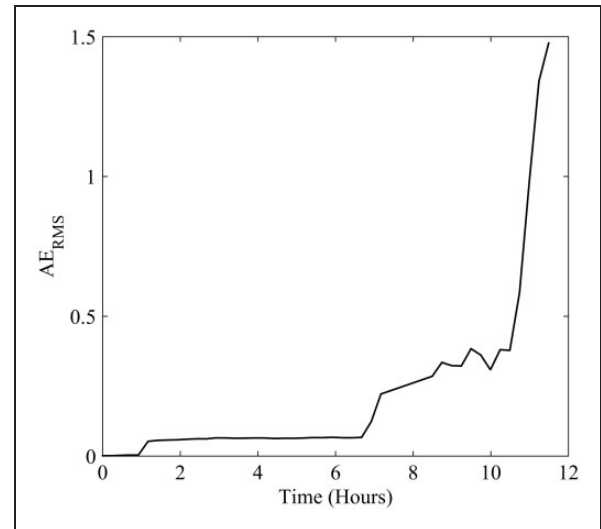


**Figure 11.** AERMS response over the duration of the bearing life test.

Following the bearing characterisation tests, in order to determine the frequency response of a bearing through end-of-life failure an accelerated life test was conducted with the load arm (and hence test bearing outer raceway) misaligned by a small degree relative to the bearing inner race in order to increase the contact stress locally within the bearing. Unlike artificial defects, natural defects tend to originate below the surface at points of high-cyclic stress due to repeated roller passes and the growth propagation relies heavily on the bearing steel's micro-structure. In the early phase of the test, the speed and load were increased gradually until a final speed and load of 5980 r/min and 2052 N, respectively, were achieved at 1.75 h after the start of the test. These test conditions remained constant until the bearing had clearly failed, with wavestreams recorded every 15 min throughout the test duration. During previous testing, it was seen that a  $\pm 10$  V transient occurred due to a suspected sub-surface crack or over-rolling of wear debris. As this experiment hoped to induce significant wear within the bearing, the pre-amplifier gain was set to 20 dB to prevent the potentially high signal levels being amplified to beyond the range of the AE system. Figure 11 plots the  $AE_{RMS}$  over the duration of the experiment. As the speed was increased over the first hour, the  $AE_{RMS}$  amplitude increases as witnessed in the previous experiments with the amplitude remaining constant once the speed was increased to 5870 r/min. Increases in load up to 1.75 h show little increase in  $AE_{RMS}$ , as it to be expected. Between the first and seventh hour, it is assumed that any bearing damage has not reached such a level that it affects relatively crude measures of signal level such as  $AE_{RMS}$ . After this time, the  $AE_{RMS}$  increases dramatically in amplitude indicating that damage levels have become more significant. Over the remaining 4 h of testing, the amplitude continues to increase until the testing was



**Figure 12.** Damage propagation on the outer and inner raceways.

stopped due to an obvious change in the audible noise of the test rig. Figure 12 shows the damage observed on both of the raceways after the rig was disassembled.

To determine if it is possible to detect the early defect growth, Figure 13 plots the frequency content of the wavestreams, versus time, with a bin width of 100 Hz, for the duration of the experiment. Figure 13(a)–(c) covers the first 7 h of testing where it is thought bearing failure is initiating, and Figure 13(d)–(f) covers the remaining period of the experiment where the bearing enters the final failure period.

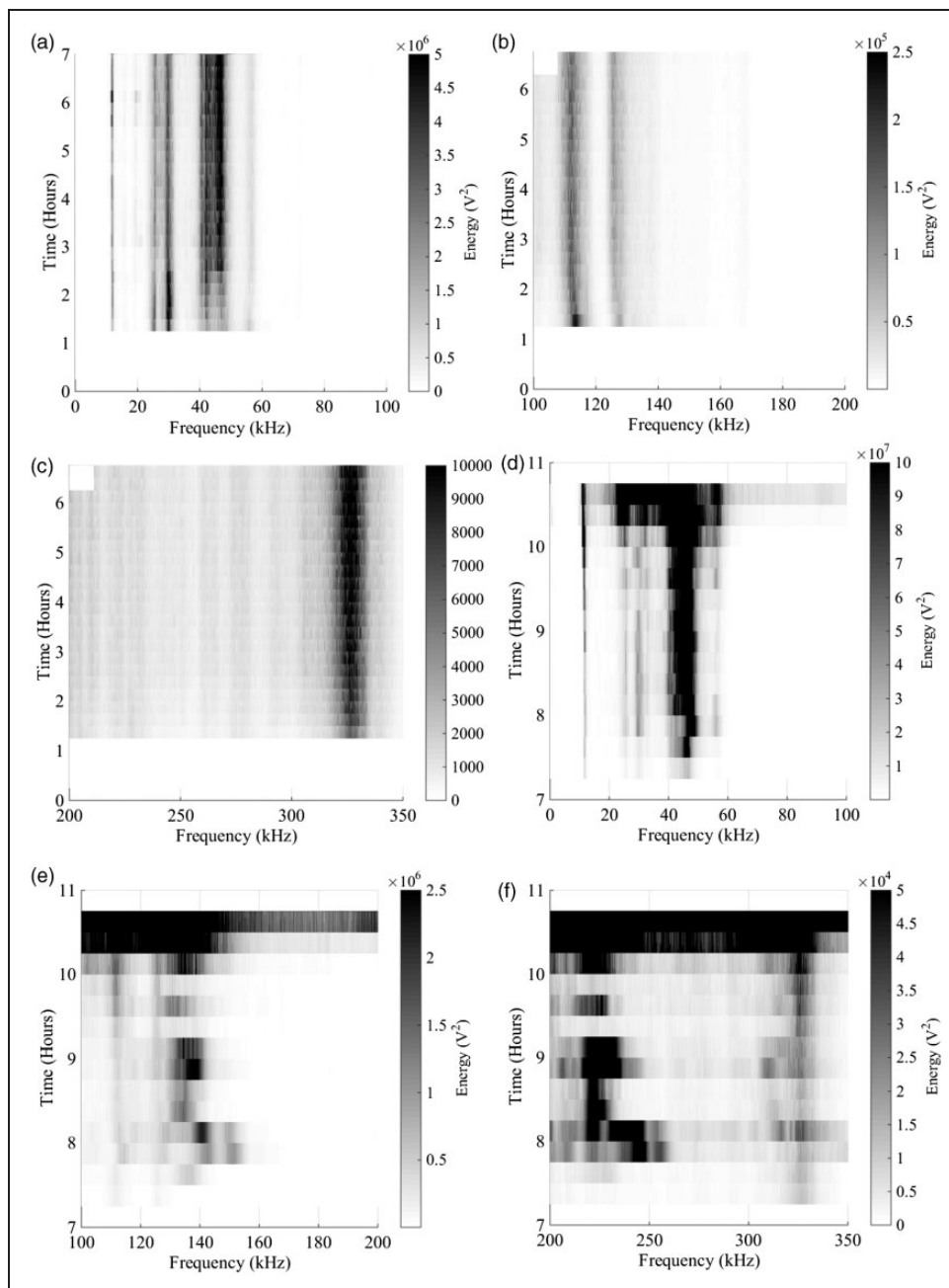


**Figure 13.** 3D binned FFT of life test wavestreams in the region between 0 and 7 h at (a) 0–100 kHz, (b) 100–200 kHz, (c) 200–350 kHz and between 7 and 11 h at (d) 0–100 kHz, (e) 100–200 kHz and (f) 200–350 kHz.

As discussed by Graney and Starry,<sup>9</sup> the HFNBRI's are excited by increasing speed as well as increasing wear and friction. Figure 13(a) shows initial high energy at 30 kHz between 1.25 and 2.5 h which then decreases in amplitude as the energy in the frequency band of 40–50 kHz begins to increase although under a constant load and speed. This increase in energy indicates an increasing change in the running conditions within the bearing and may be linked to a period of constant wear or fatigue damage accumulation. The high-frequency transients associated with increased wear and friction, between 100 and 500 kHz, remain at a continuous energy level between 1.25 and 7 h (Figure 13(b) and (c)). It is to be noted that up to 1.25 h, the amplitude of the energy is not high enough to be registered on the scale shown due to the low operational speeds. After 7 h, it is clear that the wear begins to increase rapidly, and the amplitude across all frequency bands continues to increase, although the frequencies at which they occur become far less focussed. As debris particles are released from the inner and outer raceways, multiple over-rolling events will occur, further increasing the onset of damage within the bearing. The extension of energy across a wider range of frequencies in Figure 13(e) and (f) is thought to be due to the increased number of transient energy bursts released. As more transient bursts are released, the signals produced merge together and hence lower the dominance at particular frequencies. As the bearing tends towards final failure, there exists a significant increase of energy across all frequency bands, saturating the signals produced.

## Conclusion

The speed and load applied to a bearing were investigated separately to determine their individual influence upon the recorded AE signal when operating under a full fluid film lubrication regime. Initial analysis determined a strong correlation between speed and  $AE_{RMS}$  and a far less significant effect due to increasing load. By studying the frequency response with respect to time, it was shown that the lower frequency range, 20–60 kHz, was highly sensitive to speed and is associated with the bearing's natural resonant frequencies. Whereas load has little effect on the frequencies lower than 60 kHz, the energy released at 330 kHz (the sensor's resonant frequency) increases as load is increased. It is thought that this is due to increased stresses within the contact zone and hence a greater release of strain energy and increased likelihood of plastic deformation occurring.

An accelerated life test demonstrated that during a period of continuous wear, the bearings resonant frequencies increased in amplitude even though the bearing was operating at a constant speed and load. Higher frequency components, 115, 125 and 330 kHz all remain at a constant amplitude though out the constant wear phase. As the bearing tends towards final failure, the frequencies that were previously

dominant become less so, and a broader range of frequencies become excited. It is considered that this is due to the over-rolling of multiple debris particles, causing higher frequency signals to become merged together.

The results presented here demonstrate the sensitivity of the AE technique to both bearing operating conditions, and to bearing failure, and hence demonstrate its great potential for use in bearing health monitoring systems in rotating machinery.

## Declaration of Conflicting Interests

The author(s) declared no potential conflicts of interest with respect to the research, authorship, and/or publication of this article.

## Funding

The author(s) disclosed receipt of the following financial support for the research, authorship, and/or publication of this article: The authors wish to acknowledge the support of EPSRC Grant references EP/K502819/1, EP/L021757/1 and EP/K031635/1 which facilitated this work in part. The South Wales Institute of Engineers Educational Trust (SWIET) helped to support the first author to attend the Leeds-Lyon conference to present this work. The financial support of Mistras Group Limited towards the first author's studentship is also acknowledged.

## Data access statement

Information on how to access the data that supports the results presented in this article can be found in the Cardiff University data catalogue at <http://dx.doi.org/10.17035/d.2016.0008118727>.

## References

1. García Márquez FP, Tobias AM, Pinar Pérez JM, et al. Condition monitoring of wind turbines: techniques and methods. *Renew Energy* 2012; 46: 169–178.
2. Halme J and Andersson P. Rolling contact fatigue and wear fundamentals for rolling bearing diagnostics – state of the art. *Proc IMechE, Part J: J Engineering Tribology* 2010; 224: 377–393.
3. Howard I. A review of rolling element bearing vibration 'detection, diagnosis and prognosis'. *Def Sci Technol Organ* 1994; No. DSTO-RR-00113.
4. Hase A, Mishina H and Wada M. Correlation between features of acoustic emission signals and mechanical wear mechanisms. *Wear* 2012; 292–293: 144–150.
5. Hawman MW and Galinaitis WS. Acoustic emission monitoring of rolling element bearings. In: *IEEE 1988 ultrasonics symposium proceedings*, Chicago, IL, 2–5 October 1988, pp.885–889. New York: IEEE.
6. Couturier J and Mba D. Operational bearing parameters and acoustic emission generation. *J Vib Acoust* 2008; 130: 024502.
7. Choudhury A and Tandon N. Application of acoustic emission technique for the detection of defects in rolling element bearings. *Tribol Int* 2000; 33: 39–45.
8. Williams T, Ribadeneira X, Billington S, et al. Rolling element bearing diagnostics in run-to-failure lifetime testing. *Mech Syst Signal Process* 2001; 15: 979–993.

9. Graney B and Starry K. Rolling element bearing analysis. *Mater Eval* 2012; 70: 78–85.
10. Cockerill A, Holford KM, Bradshaw T, et al. Use of high frequency analysis of acoustic emission signals to determine rolling element bearing condition. *J Phys Conf Ser* 2015; 305: 628.
11. Defence Standard 91-74:2000. Ministry of Defence.
12. Harris TA and Kotzalas MN. *Essential concepts of bearing technology*. 5th ed. Boca Raton, FL: CRC Press, 2006.
13. Hsu NN and Breckenridge FR. Characterization and calibration of acoustic-emission sensors. *Mater Eval* 1981; 39: 60–68.
14. ASTM. E976:2010. A standard guide for determining the reproducibility of acoustic emission sensor response.
15. Dowson D and Higginson GR. *Elasto-hydrodynamic lubrication: international series on materials science and technology*. New York: Elsevier, 2014, p.250.
16. NSK Europe. Protect your bearing investment: proper run-in procedures help to maximise bearing life, 2015. Available at: [http://www.nskeurope.com/cps/rde/dtr/eu\\_es/literature\\_bearing/EN\\_Technical-Insight\\_Protect-Bearing-Investment.pdf](http://www.nskeurope.com/cps/rde/dtr/eu_es/literature_bearing/EN_Technical-Insight_Protect-Bearing-Investment.pdf).
17. Lees AW, Quiney Z, Ganji A, et al. The use of acoustic emission for bearing condition monitoring. *J Phys Conf Ser* 2011; 305: 012074.
18. Pullin R, Clarke A, Eaton MJ, et al. Identification of the onset of cracking in gear teeth using acoustic emission. *J Phys Conf Ser* 382: 012050.